Parametric Channel Estimation and Design for Active-RIS-Assisted Communications

Md. Shahriar Sadid, Ali A. Nasir, Saad Al-Ahmadi, and Samir Al-Ghadhban

Abstract—Reconfigurable Intelligent Surface (RIS) technology has emerged as a key enabler for future wireless communications. However, its potential is constrained by the difficulty of acquiring accurate user-to-RIS channel state information (CSI), due to the cascaded channel structure and the high pilot overhead of non-parametric methods. Unlike a passive RIS, where the reflected signal suffers from multiplicative path loss, an active RIS amplifies the signal, improving its practicality in real deployments. In this letter, we propose a parametric channel estimation method tailored for active RISs. The proposed approach integrates an active RIS model with an adaptive Maximum Likelihood Estimator (MLE) to recover the main channel parameters using a minimal number of pilots. To further enhance performance, an adaptive active RIS configuration strategy is employed, which refines the beam direction based on an initial user location estimate. Moreover, an orthogonal anglepair codebook is used instead of the conventional Discrete Fourier Transform (DFT) codebook, significantly reducing the codebook size and ensuring reliable operation for both far-field and nearfield users. Extensive simulations demonstrate that the proposed method achieves near-optimal performance with very few pilots compared to non-parametric approaches. Its performance is also benchmarked against that of a traditional passive RIS under the same total power budget to ensure fairness. Results show that active RIS yields higher spectral efficiency (SE) by eliminating the multiplicative fading inherent in passive RISs and allocating more resources to data transmission.

Index Terms—Active Reconfigurable Intelligent Surface, Channel Estimation, MLE.

I. INTRODUCTION

Next-generation (6G) wireless networks require innovations that reconfigure the propagation environment to improve end-to-end performance. Reconfigurable intelligent surfaces (RISs) have emerged as a promising means of enhancing wireless channels via programmable metasurfaces [1]. A conventional passive RIS comprises many low-cost, passive scatterers that reflect incident signals with adjustable phase shifts, thereby shaping the channel without additional transmit power [2]. However, passive RISs intrinsically suffer from a double-fading (multiplicative path-loss) effect: the end-to-end gain factors as the product of the transmitter-to-RIS and RIS-to-

Md. Shahriar Sadid, Ali A. Nasir, Saad Al-Ahmadi, and Samir Al-Ghadhban are with the Department of Electrical Engineering, King Fahd University of Petroleum and Minerals (KFUPM), Dhahran 31261, Saudi Arabia. They are also affiliated with the Center for Communication Systems and Sensing at KFUPM. This work was supported by KFUPM, IRC-CSS Center, under project number INCS2406. (email: g202313670@kfupm.edu.sa, anasir@kfupm.edu.sa, saadbd@kfupm.edu.sa, samir@kfupm.edu.sa).

receiver gains, so the reflected signal experiences attenuation twice [3].

To overcome this limitation, researchers have proposed active RIS (ARIS) architectures in which each element integrates active components (e.g., low-power amplifiers or transceiver chips) that amplify rather than merely reflect the impinging wave [3]. By providing extra power at the surface, an active RIS can compensate for double-path loss, effectively converting multiplicative attenuation into an additive gain term in the link budget. Recent works have shown that active RIS can outperform their passive counterparts under comparable settings [1], [4]. In this sense, the active RIS concept can be viewed as a natural evolution of the traditional RIS, using a small amount of surface power to counter the effects of double fading and boost overall network throughput [1].

Even with these advantages, obtaining accurate channel state information (CSI) in RIS-aided systems is still a difficult problem. In typical RIS deployments, the base station (BS) does not observe the constituent links directly; instead, it measures a cascaded channel—the product of the user-to-RIS and RIS-to-BS channels—modulated by the RIS elements' responses [5].

Moreover, the classical far-field assumption (planar wave-fronts) may not hold for large-aperture RISs that operate in the near field, where spherical wavefront propagation must be modeled. In this regime, the channel depends not only on angular direction but also on the distance to each RIS element, introducing additional parameters [6]. Near-field channels offer higher spatial degrees of freedom. However, they substantially increase the complexity of channel modeling and estimation. Consequently, far-field (angle-only) parameterizations become inaccurate in the near field or require an excessive number of pilots [6].

Mylonopoulos *et al.* [7] derived a maximum-likelihood estimator (MLE) for user position and orientation in a mmWave network with an active RIS, treating the line-of-sight (LoS) paths via the RIS as geometric signals and using maximum likelihood to infer location with high accuracy. Although their objective—localization—differs from ours, the result reinforces that MLE on parametric LoS channel models (angles and distances) is effective, and that active RIS hardware can further enhance estimation. Chen *et al.* [8] investigated channel estimation and training design for active RIS-aided systems in which each RIS element can amplify the reflected signal. A Cramér–Rao lower bound (CRLB) analysis shows that active amplification can reduce pilot overhead relative to passive RISs, albeit at the expense of increased noise. This early

contribution proposed joint training and least-squares (LS) estimation that exploits amplification to improve estimation performance and provides insight into reflection-coefficient design. Dynamic channel tracking has recently been investigated in the context of active RISs. Haider *et al.* [9] proposed a semi-passive RIS architecture to handle time-varying channels (e.g., due to user mobility) while maintaining low pilot overhead. In their design, only a small subset of RIS elements are active (equipped with RF chains) and intermittently sense the channel. A long short-term memory (LSTM) network is then employed for temporal prediction; however, it requires a training phase and performs reliably only when user mobility patterns resemble those represented in the training data.

Another emerging direction employs machine learning to design efficient training protocols for active RISs. Zhang and Yu [10] developed an adaptive beamforming codebook for active RIS-aided localization; unlike conventional beam training, their approach learns codebook construction and beam selection. However, generalization may degrade when the deployment environment or hardware differs from the training data, necessitating retraining. Moreover, executing an LSTM-based selection loop in real time increases controller complexity, as it must perform on-the-fly neural inference.

In this letter, we exploit the signal-amplification capability of active reconfigurable intelligent surfaces (ARISs) to tackle the challenging problem of channel estimation. We develop a parametric maximum likelihood estimation (MLE) framework and derive closed-form expressions for all channel parameters under both near-field and far-field conditions.

Compared with passive RISs, channel estimation for active RISs is complicated by two key factors: (i) amplified thermal and phase noise, which obscures parameter identification, and (ii) practical implementation requirements, as each active element demands precise calibration of both phase and amplitude. We address these challenges with a methodology tailored to the active RIS architecture that jointly estimates the amplitude and phase components of the channel response. The proposed framework delivers closed-form localization parameters—angles for far-field users and angles plus distance for near-field users—and includes a beamforming design specifically adapted to active RIS hardware.

A central feature of the framework is an adaptive pilot-selection mechanism that dynamically allocates pilots to the most informative directions as estimation proceeds, improving accuracy without increasing pilot overhead. To the best of our knowledge, this is the first comprehensive parametric estimation solution explicitly designed for the amplification and noise characteristics of active RISs, and it operates seamlessly across both near-field and far-field regimes.

II. SYSTEM AND CHANNEL MODEL

We consider an uplink system comprising a single-antenna base station (BS) and a single-antenna user equipment (UE) assisted by an active reconfigurable intelligent surface (ARIS). No direct BS-to-UE link is assumed. The active RIS comprises N elements with independently tunable amplitude and phase. We model the BS-to-ARIS channel, $\boldsymbol{h} \in \mathbb{C}^N$, as a deterministic Line-of-Sight (LoS) link. Given that the BS and active RIS are fixed in location, this channel is considered quasi-stationary and non-fading over the signaling interval. The ARIS-to-UE channel is $\boldsymbol{g} \triangleq [g_1,\ldots,g_N]^{\mathrm{T}} \in \mathbb{C}^N$, which is time varying due to user mobility. To maintain a high signal-to-noise ratio (SNR), the BS periodically estimates the channel and updates the active RIS coefficients (phase shifts and gains) accordingly.

Let the UE transmit the symbol $x \sim \mathcal{CN}(0, P_d)$. The received signal at the BS is

$$y = (\mathbf{\Phi}^{\mathrm{T}} \mathbf{D}_{h} \mathbf{g}) x + \mathbf{\Phi}^{\mathrm{T}} \mathbf{D}_{h} \mathbf{v} + w, \tag{1}$$

where $\Phi \triangleq [\phi_1,\ldots,\phi_N]^{\mathrm{T}}$, it collects the complex active RIS coefficients (per-element gain and phase). Here $\mathbf{D}_h = \mathrm{diag}(h_1,\ldots,h_N)$, and $\Phi_n = p_n e^{\mathrm{j}\theta_n}$ is the active RIS configuration, where θ_n is the phase shift and p_n is the amplification factor of the nth element, respectively.

Two noise components are present: the active RIS amplification noise, $\boldsymbol{v} \sim \mathcal{CN}(\mathbf{0}_N, \sigma_v^2 \mathbf{I}_N)$, and the receiver noise, $\boldsymbol{w} \sim \mathcal{CN}(0, \sigma^2)$.

The spectral efficiency (SE) can be expressed as

$$R = \log_2 \left(1 + \frac{P_d \left| \mathbf{\Phi}^{\mathrm{T}} \mathbf{D}_h \mathbf{g} \right|^2}{\sigma^2 + \left\| \mathbf{\Phi}^{\mathrm{T}} \mathbf{D}_h \right\|_2^2 \sigma_v^2} \right). \tag{2}$$

The line-of-sight (LoS) channel vector from UE-to-ARIS is modeled as

$$\mathbf{g} = \sqrt{\beta} e^{j\omega} \mathbf{a}(\psi) \tag{3}$$

where $\beta \geq 0$ and $\omega \in [0,2\pi)$ denote, respectively, the channel gain and the phase referenced to the first active RIS element, and $a(\psi)$ is the array-response vector parameterized by ψ . This model applies to both near- and far-field propagation: in the far field, $\psi = (\varphi, \phi)$ comprises the azimuth φ and elevation ϕ ; in the near field, $\psi = (\varphi, \phi, r)$ additionally includes the distance r from the UE to the first active RIS element.

For the near field, the array-response vector can be written as [11]

$$\mathbf{a}(\varphi, \phi, r) = \left[1, e^{j\frac{2\pi}{\lambda}s_2}, e^{j\frac{2\pi}{\lambda}s_3}, \dots, e^{j\frac{2\pi}{\lambda}s_N}\right]^{\mathrm{T}}, \tag{4}$$

where $s_n \triangleq r_n - r_1$ denotes the path-length difference between the nth element and the reference (first) element, with r_n being the distance from the UE to the nth active RIS element.

In the far field, the response reduces to the conventional planar-wave form [12]

$$\mathbf{a}(\varphi,\phi) = \left[1, \dots, e^{j\frac{2\pi}{\lambda}(i(n)\sin\varphi\cos\phi + k(n)\sin\phi)}, \dots, e^{j\frac{2\pi}{\lambda}((N_{\mathrm{H}} - 1)\Delta_{\mathrm{H}}\sin\varphi\cos\phi + (N_{\mathrm{V}} - 1)\Delta_{\mathrm{V}}\sin\phi)}\right]_{,}^{\mathrm{H}},$$
(5)

where i(n) and k(n) are the horizontal and vertical coordinates (index positions) of the nth active RIS element, Δ_H and Δ_V are the inter-element spacings along the horizontal and vertical axes, and N_H and N_V denote the numbers of elements per row and column, respectively. We can express i(n) and k(n) in terms of Δ_H and Δ_V [12],

$$i(n) = (n_H - 1)\Delta_H, \quad k(n) = (n_V - 1)\Delta_V,$$

where,

$$n_H = \operatorname{mod}(n-1, N_H) + 1, \quad n_V = \left\lceil \frac{n}{N_H} \right\rceil.$$

III. MLE-BASED ESTIMATION FOR ACTIVE RIS

We consider the received-signal model when the UE transmits a pilot symbol as

$$\mathbf{y} = (\mathbf{B} \mathbf{D}_h \mathbf{g}) \sqrt{P_p} + \mathbf{B} \mathbf{D}_h \mathbf{v} + \mathbf{w}, \tag{6}$$

where $\boldsymbol{y} \in \mathbb{C}^L$ is the received vector across L pilot instances, $\boldsymbol{B} \in \mathbb{C}^{L \times N}$ is the active RIS configuration matrix over these instances, P_p is the pilot power. We are sending the same pilot but for L slots.

The deterministic mean is $\mu(g) = (B D_h g) \sqrt{P_p}$, and the effective noise is $\tilde{w} = B D_h v + w$; $\tilde{w} \sim \mathcal{CN}(0, F)$, with total noise covariance

$$\mathbf{F} = \sigma^2 \mathbf{I}_L + \sigma_v^2 \mathbf{B} \mathbf{D}_h \mathbf{D}_h^{\mathrm{H}} \mathbf{B}^{\mathrm{H}}. \tag{7}$$

The Maximum Likelihood (ML) estimate of the channel g, denoted by \hat{g} , is the argument that maximizes the likelihood function of the received signal vector y. The likelihood function $f_Y(y;g)$ is given by

$$f_{\mathbf{Y}}(\mathbf{y}; \mathbf{g}) = \frac{1}{\pi^{L} \det(\mathbf{F})} \exp\left(-\left(\mathbf{y} - \boldsymbol{\mu}(\mathbf{g})\right)^{H} \mathbf{F}^{-1} \left(\mathbf{y} - \boldsymbol{\mu}(\mathbf{g})\right)\right)$$
(8)

Maximizing the likelihood $f_Y(y;g)$ is equivalent to minimizing the quadratic form in the exponent. Since F is Hermitian positive definite, F^{-1} is Hermitian. Therefore,

$$(y - \mu(g))^{H} F^{-1}(y - \mu(g))$$

$$= y^{H} F^{-1} y - y^{H} F^{-1} \mu(g) - \mu^{H}(g) F^{-1} y + \mu^{H}(g) F^{-1} \mu(g)$$

$$= y^{H} F^{-1} y - 2 \Re \left\{ y^{H} F^{-1} \mu(g) \right\} + \mu^{H}(g) F^{-1} \mu(g)$$

$$= y^{H} F^{-1} y - 2 \sqrt{P_{p}} \Re \left\{ y^{H} F^{-1}(B \mathbf{D}_{h} g) \right\}$$

$$+ P_{p} (B \mathbf{D}_{h} g)^{H} F^{-1} (B \mathbf{D}_{h} g).$$
(0)

The constant term $y^H F^{-1}y$ can be discarded as it does not depend on g and thus does not affect its estimation. Hence,

$$\hat{\boldsymbol{g}} = \underset{\boldsymbol{g}}{\operatorname{arg\,min}} \left[-2\sqrt{P_p} \,\Re \left\{ \boldsymbol{y}^{\mathrm{H}} \boldsymbol{F}^{-1} \mathbf{B} \mathbf{D}_h \boldsymbol{g} \right\} + P_p \left(\mathbf{B} \mathbf{D}_h \boldsymbol{g} \right)^{\mathrm{H}} \boldsymbol{F}^{-1} (\mathbf{B} \mathbf{D}_h \boldsymbol{g}) \right]. \tag{10}$$

Now substitute $\mathbf{g} = \sqrt{\beta} e^{j\omega} \mathbf{a}(\psi)$:

$$\{\hat{\beta}, \hat{\omega}, \hat{\psi}\} = \underset{\beta \geq 0, \, \omega \in [0, 2\pi)}{\operatorname{arg \, min}} \left[P_{p} \beta \, \boldsymbol{a}(\boldsymbol{\psi})^{H} \mathbf{D}_{h}^{H} \mathbf{B}^{H} \boldsymbol{F}^{-1} \mathbf{B} \mathbf{D}_{h} \boldsymbol{a}(\boldsymbol{\psi}) - 2 \sqrt{P_{p} \beta} \, \Re \left\{ e^{j\omega} \, \boldsymbol{y}^{H} \boldsymbol{F}^{-1} \mathbf{B} \mathbf{D}_{h} \boldsymbol{a}(\boldsymbol{\psi}) \right\} \right].$$

$$(11)$$

A. ARIS Reflected Channel Phase (ω)

The expression in (11) is minimized when the real part inside the objective is maximized. Therefore, the optimal phase $\hat{\omega}$ aligns the exponential term with the phase of the complex inner product.

$$\hat{\omega} = -\arg\{\mathbf{y}^{\mathrm{H}}\mathbf{F}^{-1}\mathbf{B}\mathbf{D}_{h}\boldsymbol{a}(\psi)\}. \tag{12}$$

Now, by substituting the value of $\hat{\omega}$ into the equation (11) , we get

$$\{\hat{\beta}, \ \hat{\boldsymbol{\psi}}\} = \underset{\boldsymbol{\psi} \in \Psi}{\operatorname{arg\,min}} \left[P_{p} \beta \left(\boldsymbol{a}(\boldsymbol{\psi})^{H} \mathbf{D}_{h}^{H} \mathbf{B}^{H} \mathbf{F}^{-1} \mathbf{B} \mathbf{D}_{h} \boldsymbol{a}(\boldsymbol{\psi}) \right) - 2 \sqrt{P_{p}} \sqrt{\beta} \left| \mathbf{y}^{H} \mathbf{F}^{-1} \mathbf{B} \mathbf{D}_{h} \boldsymbol{a}(\boldsymbol{\psi}) \right| \right].$$

$$(13)$$

B. ARIS Reflected Channel Amplitude (β)

This is a quadratic function in terms of $\sqrt{\beta}$, for which the minimizer can be determined in closed form as

$$\hat{\beta} = \frac{\left| \mathbf{y}^{\mathrm{H}} \mathbf{F}^{-1} \mathbf{B} \mathbf{D}_{h} \mathbf{a}(\psi) \right|^{2}}{P_{p} \left(\mathbf{a}(\psi)^{\mathrm{H}} \mathbf{D}_{h}^{\mathrm{H}} \mathbf{B}^{\mathrm{H}} \mathbf{F}^{-1} \mathbf{B} \mathbf{D}_{h} \mathbf{a}(\psi) \right)^{2}}.$$
 (14)

C. ARIS Reflected Channel Array Response Parameter (ψ)

By replacing this value $\hat{\beta}$ in equation (13), we get:

$$\hat{\psi} = \underset{\psi \in \Psi}{\operatorname{arg\,max}} \frac{\left| \mathbf{y}^H \mathbf{F}^{-1} \mathbf{B} \mathbf{D}_h \mathbf{a}(\psi) \right|^2}{\mathbf{a}(\psi)^H \mathbf{D}_h^H \mathbf{B}^H \mathbf{F}^{-1} \mathbf{B} \mathbf{D}_h \mathbf{a}(\psi)}.$$
 (15)

IV. ADAPTIVE BEAM AND AMPLIFICATION FACTOR

We employ an orthogonal angle-based codebook in place of the conventional DFT codebook. Let $\Theta = \{\theta_k \in \mathbb{C}^N : \|\theta_k\|_{\infty} = 1, \ k = 1, \ldots, K\}$ collect unit-modulus, phase-only beams generated from orthogonal angle pairs (far field: (φ, ϕ) ; near field: (φ, ϕ, r)). By construction, $\theta_i^H \theta_j \approx 0$ for $i \neq j$, so the search space contracts from an $N \times N$ DFT matrix to $R \ll N^2$ nearly orthogonal beams, each column representing a single active RIS configuration direction.

Initialization via wide-beam probing

Rather than selecting an arbitrary codebook column, we first form two wide beams that cover complementary sectors ([13] section VI). Let $\theta_{w,1}$ and $\theta_{w,2}$ denote the two unit-modulus phase vectors. Each vector is configured to generate a wide

beam covering a distinct angular region on either side of the active RIS, facilitating initial user discovery. The initial active RIS coefficients apply equal per-element gain with phases from the wide beams,

$$\phi_1 = \sqrt{\frac{P_{\text{RIS}}}{N}} \boldsymbol{\theta}_{w,1}, \qquad \phi_2 = \sqrt{\frac{P_{\text{RIS}}}{N}} \boldsymbol{\theta}_{w,2}, \qquad (16)$$

Here, ϕ_1 and ϕ_2 are the initial active RIS configurations. The matrix **B** initially contains only these two configurations. Each time a pilot is transmitted, the newly selected active RIS configuration is appended to B as an additional row. These pilots reliably illuminate the UE in both near- and far-field regimes and significantly reduce the required pilot count in the first step.

Active-RIS amplitude shaping and phase alignment:

Given \hat{g} , we design the per-element phases for coherent combining across the cascaded links:

$$\bar{\boldsymbol{\theta}}^{\mathrm{opt}} = \exp(-\mathrm{j} \angle(\mathbf{D}_h \widehat{\boldsymbol{g}})),$$
 (17)

which cancels the aggregate phase $h_n \widehat{g}_n$ at each element. The per-element amplification vector p is then computed in closed form under the active RIS power constraint using [14, Sec. V, Cor. 3] given by,

$$p_n^{\text{(est)}} = C \frac{\alpha_n}{\beta_n + \gamma_n}, \tag{18}$$

where,

$$\alpha_n = |\widehat{g}_n| |h_n|, \qquad \beta_n = |h_n|^2, \qquad \gamma_n = \frac{|\widehat{g}_n|^2 \frac{p_d}{\sigma_v^2} + 1}{\frac{P_{\text{ris}}}{\sigma^2}},$$

$$C = \left(\sum_{n=1}^{N} \frac{|\alpha_n|^2 \gamma_n}{(\beta_n + \gamma_n)^2}\right)^{-1/2}.$$

For the initial pilots, the channel is unknown; therefore, this amplification factor cannot be applied. After processing initial pilots and obtaining a channel estimate, we update the amplification factor in the next active RIS configuration. The resulting active RIS configuration, ϕ^* is then used for pilot transmission, which is

$$\phi^{\star} = \boldsymbol{p}^{(\text{est})} \odot \bar{\boldsymbol{\theta}}^{\text{opt}},$$
 (20)

where \odot denotes the Hadamard product.

Adaptive pilot selection via the closest-beam rule:

To refine the estimate with additional pilots, we choose the next phase-only codeword by maximizing its alignment with the current active vector:

$$\boldsymbol{\theta}^{\text{next}} = \arg \max_{\boldsymbol{\theta} \in \boldsymbol{\Theta}} | (\boldsymbol{\phi}^{\star})^{\text{H}} \boldsymbol{\theta} |.$$
 (21)

Here $heta^{ ext{next}}$ is the phase-only active RIS setting for the next pilot. The corresponding active RIS vector is

$$\phi_{\text{new}} = \boldsymbol{p}^{(\text{est})} \odot \boldsymbol{\theta}^{\text{next}}.$$
 (22)

Algorithm 1 Parametric MLE for near/far field with active RIS and adaptive pilots

1: **Input:** $\mathbf{D}_h = \operatorname{diag}(\mathbf{h})$, codebook $\boldsymbol{\Theta}$ (phase-only), initial configurations $\{\theta_{w,1}, \theta_{w,2}\}$, number of slots L, powers P_p , P_d , P_{RIS}

2: Initialization: Set
$$\mathbf{D}_{h, \angle} \leftarrow \operatorname{diag}(\mathbf{h}/|\mathbf{h}|)$$

 $\boldsymbol{\phi}_1 \leftarrow \sqrt{P_{\mathrm{RIS}}/N} \, \boldsymbol{\theta}_{w,1}, \quad \boldsymbol{\phi}_2 \leftarrow \sqrt{P_{\mathrm{RIS}}/N} \, \boldsymbol{\theta}_{w,2}$
3: $\mathbf{B}_2 \leftarrow [\boldsymbol{\phi}_1, \boldsymbol{\phi}_2]^\top, \quad \mathbf{y}_2 \in \mathbb{C}^2$

4: for $\ell = 2$ to L do

 $\begin{aligned} \mathbf{y}_{\ell} &= \sqrt{P_p} \mathbf{B}_{\ell} \mathbf{D}_h \mathbf{g} + \mathbf{v}_{\ell} + \mathbf{w}_{\ell} \\ \text{where } [\mathbf{v}_{\ell}]_i &= \mathbf{B}_{\ell}(i,:) \mathbf{D}_h \mathbf{v}_i \\ \text{Compute closed-form MLE:} \end{aligned}$

6:

$$\hat{\psi}_{\ell} = rg \max_{oldsymbol{\psi} \in \Psi} rac{\left| \mathbf{y}^H \mathbf{F}^{-1} \mathbf{B} \mathbf{D}_h oldsymbol{a}(oldsymbol{\psi})
ight|^2}{oldsymbol{a}(oldsymbol{\psi})^H \mathbf{D}_h^H \mathbf{B}^H \mathbf{F}^{-1} \mathbf{B} \mathbf{D}_h oldsymbol{a}(oldsymbol{\psi})}$$

Obtain $\hat{\beta}_{\ell}$, $\hat{\omega}_{\ell}$ from (14) and (12) and set $\hat{\mathbf{g}}_{\ell}$ accord-7: ing to (3)

Active RIS amplitude shaping: for $k=1,\ldots,N$ Compute $p_k^{(\mathrm{est})}=C\frac{\alpha_k}{\beta_k+\gamma_k}$ if $\ell < L$ then 8:

9:

10:

$$\bar{\boldsymbol{\theta}}_{\ell}^{\mathrm{opt}} = \exp\left(-j \angle (\mathbf{D}_{h}\hat{\mathbf{g}}_{\ell})\right), \quad \boldsymbol{\phi}_{\ell}^{\star} = \mathbf{p}^{(\mathrm{est})} \odot \bar{\boldsymbol{\theta}}_{\ell}^{\mathrm{opt}}$$

11: Select next pilot via:

$$\boldsymbol{\theta}_{\ell+1} = \arg\max_{\boldsymbol{\theta} \in \boldsymbol{\Theta}} \left| (\boldsymbol{\phi}_{\ell}^{\star})^{\mathrm{H}} \boldsymbol{\theta} \right|$$

12: Update:

$$oldsymbol{\phi}_{ ext{new}} = \mathbf{p}^{(ext{est})} \odot oldsymbol{ heta}_{\ell+1}, \quad \mathbf{B}_{\ell+1} = egin{bmatrix} \mathbf{B}_{\ell} \ oldsymbol{\phi}_{ ext{new}}^{ op} \end{bmatrix}, \ oldsymbol{\Theta} \leftarrow oldsymbol{\Theta} \setminus \{oldsymbol{ heta}_{\ell+1}\}.$$

13: Transmit pilot $\ell+1$ and collect $\mathbf{y}_{\ell+1}$

14: end if

15: end for

(19)

16: Output: $\hat{\mathbf{g}} = \hat{\mathbf{g}}_L$

We append ϕ_{new} as a new row to the configuration matrix **B**, collect the corresponding measurement, and update \hat{q} via the MLE step. This greedy closest-beam procedure repeats until the pilot budget is exhausted. After selecting a configuration from the codebook Θ , it is removed from further consideration.

Remarks on complexity and applicability:

At each refinement, we evaluate the remaining phase-only codewords in the codebook. Let Θ_{rem} denote the unused set of RIS configuration after the two initial pilots. Each iteration computes $|\Theta_{\text{rem}}|$ inner products of length N, giving a periteration complexity of $\mathcal{O}(N|\Theta_{\text{rem}}|)$. With L instances of the pilot and total codebook size R (with $R \ll N^2$), the overall training cost scales as $\mathcal{O}(LNR)$, which is substantially lower than DFT-based exhaustive search. The procedure is agnostic to the propagation regime: only the steering parameterization ψ changes—angles in the far field, and angles plus distance in the near field—while the MLE and adaptive-pilot logic remain

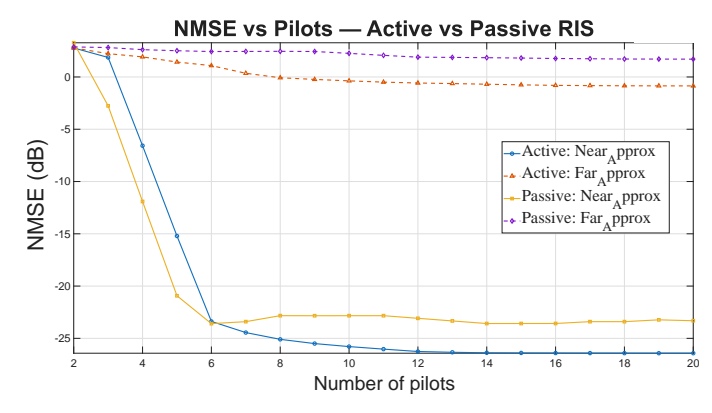


Fig. 1: NMSE (Near-field)

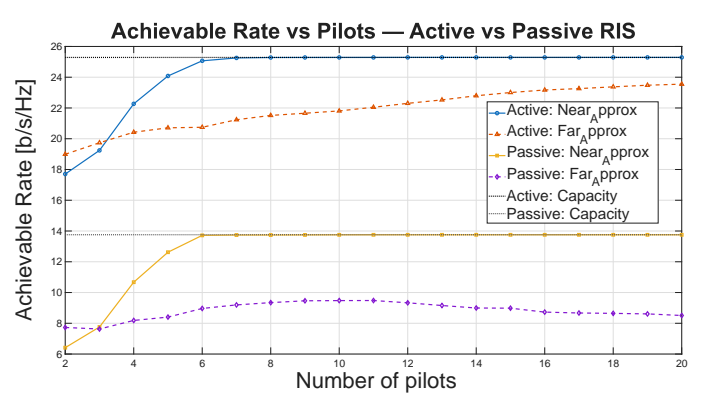


Fig. 2: Rate (Near-field)

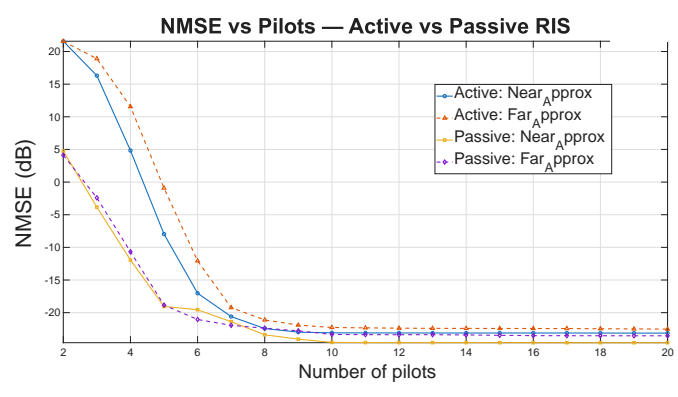


Fig. 3: NMSE (Far-field)

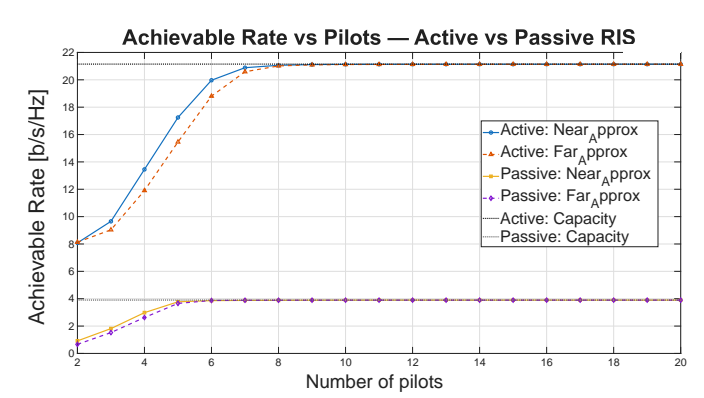


Fig. 4: Rate (Far-field)

the same.

V. SIMULATION RESULTS ANALYSIS

We evaluate the proposed estimator's performance through Monte Carlo simulations. The system operates at a carrier frequency of 28 GHz with a 1 MHz bandwidth and consists of a single-antenna base station (BS) and user equipment (UE) assisted by an active reconfigurable intelligent surface (ARIS). The active RIS is a uniform planar array of 32×32 elements with half-wavelength spacing ($\Delta_H = \Delta_V = \lambda/2$), positioned 15 m from the BS.

The users are randomly distributed with azimuth and elevation angles drawn from $\phi, \varphi \sim \mathcal{U}[-\pi/3, \pi/3]$. We distinguish between near- and far-field scenarios based on the Fraunhofer distance, $d_{\rm f}=2D^2/\lambda$, where D is the largest physical aperture dimension. For the near-field, the user distance r is sampled from $\mathcal{U}[d_{\rm B}, d_{\rm f}/10]$, where $d_{\rm B}=2D$ denotes the Björnson distance [15]. For the far-field, the distance is drawn from $\mathcal{U}[d_{\rm f}, 5d_{\rm f}]$. The pilot transmission power is set 10 dB above the data power.

To validate the effectiveness of the active architecture, the proposed scheme is benchmarked against a conventional passive RIS. The most crucial aspect of this comparison is maintaining a fair total power budget. For the passive RIS scenario, the entire power budget is dedicated to the BS

transmission. On the other hand, for the active RIS scenario, 25% of the total power is allocated to the RIS's internal amplifiers. Consequently, the BS transmits power in the active RIS-assisted system is limited to the remaining 75% of the total budget, ensuring an equitable comparison between the two architectures. 200~mW is set for the total power. The presented results are averaged over 1000~independent channels and noise realizations.

For the case of the user being in the near field, the active RIS achieves a final NMSE that is considerably lower by several dB than the minimum NMSE achieved by the passive RIS structure. This behavior is being observed under both the near and far field approximations. In contrast, for the case of the user being in the far field, both these architectures portray almost equivalent behavior under both approximation models.

The rate curves in Figs. 4 and 2 represent the theoretical capacity limits as well as the pilots achievable rate. It consistently shows higher values for the active RIS compared to the passive RIS for all the pilots. Crucially, the operational rate of the active RIS closely approaches its capacity bound, whereas the passive RIS operates well below that of the active RIS, reflecting a much lower capacity ceiling. In the nearfield case, the active RIS achieves 25.2858 bps/Hz, while the passive RIS reaches only 13.7580 bps/Hz. This gap becomes even more pronounced in the far-field scenario, where the active RIS attains 24.5325 bps/Hz, nearly three times higher

than the passive RIS's 8.6790 bps/Hz, under identical pilot configurations. These results clearly indicate that the active RIS not only enables more accurate channel estimation but also substantially enhances the achievable data rate of the overall communication system.

A key observation is, when the user is located in the far field, both approximation models provide accurate results. However, in the near field, the far-field approximation becomes less effective. The performance gap in the active RIS case remains minimal— a difference of 1.7392 bps/Hz—whereas for the passive RIS case, it widens significantly to 5.2515 bps/Hz, reaffirming the superiority of the active RIS architecture.

For any fixed number of pilots, the achievable rate of the active RIS is consistently and markedly higher than that of its passive counterpart. This highlights the pilot efficiency of the active RIS: it requires considerably fewer training resources to achieve near-optimal performance, thereby reserving more channel uses for data transmission and improving overall spectral efficiency.

These findings validate the efficacy of employing active RIS for channel estimation. Importantly, this performance gain is realized under a fair total power budget, with the active RIS system consuming less transmit power at the base station. These results demonstrate that allocating a fraction of the system's power budget to the RIS for signal amplification is far more beneficial than concentrating all power at the transmitter in a passive setup. By effectively overcoming the double-path-loss effect, the active RIS emerges not merely as a viable alternative but as a superior paradigm for achieving high-reliability, high-efficiency wireless communication.

VI. CONCLUSION

Giving every RIS element its own amplifier fundamentally changes the trade-offs relative to passive designs. By converting multiplicative path loss into net link gain, active RIS can increase capacity and efficiency in 6G networks. The future of the wireless network depends on practical scenarios of hardware implementation, such as the nonlinearity of amplifiers, tight power budgets, and calibration drift. Some semi-RIS architectures, where some elements act as active and others as passive, are also worth exploring by using sparse sensing with adaptive gain control to scale wideband estimation. For the future, the most important thing should be building hybrid approaches that focus not only on the bending of modelbased reasoning but also on data-driven learning approaches. It will then be easily adaptable to the user's mobility and in cases of channel's blockage while remaining within the limits of thermal and power constraints. If the designs of the codebooks, algorithms, and hardware are integrated, they will deliver many meaningful results in terms of both spectral and energy efficiency for the upcoming rise of the active RIS in the next generation of wireless networks.

REFERENCES

- [1] Z. Zhang, L. Dai, X. Chen, C. Liu, F. Yang, R. Schober, and H. V. Poor, "Active ris vs. passive ris: Which will prevail in 6g?" *IEEE Transactions on Communications*, vol. 71, no. 3, p. 1707–1725, Mar. 2023. [Online]. Available: http://dx.doi.org/10.1109/TCOMM.2022.3231893
- [2] M. A. ElMossallamy, H. Zhang, L. Song, K. G. Seddik, Z. Han, and G. Y. Li, "Reconfigurable intelligent surfaces for wireless communications: Principles, challenges, and opportunities," *IEEE Transactions on Cognitive Communications and Networking*, vol. 6, no. 3, pp. 990–1002, 2020
- [3] M. Khoshafa, T. Ngatched, M. H. Ahmed, and A. R. Ndjiongue, "Active reconfigurable intelligent surfaces-aided wireless communication system," *IEEE Communications Letters*, vol. PP, pp. 1–1, 09 2021.
- [4] R. Long, Y.-C. Liang, Y. Pei, and E. G. Larsson, "Active reconfigurable intelligent surface-aided wireless communications," *IEEE Transactions* on Wireless Communications, vol. 20, no. 8, pp. 4962–4975, 2021.
- [5] A. Dkhan, S. Tarboush, H. Sarieddeen, and T. Y. Al-Naffouri, "Risaided near-field channel estimation under mutual coupling and spatial correlation," arXiv preprint arXiv:2508.01828, 2025.
- [6] W.-X. Long, S. Ye, M. Moretti, M. Morelli, L. Sanguinetti, R. Chen, and C.-X. Wang, "Channel estimation for 6g near-field wireless communications: A comprehensive survey," arXiv preprint arXiv:2507.23526, 2025.
- [7] G. Mylonopoulos, L. Venturino, S. Buzzi, and C. D'Andrea, "Maximum-likelihood user localization in active-ris empowered mmwave wireless networks," in 2023 17th European Conference on Antennas and Propagation (EuCAP), 2023, pp. 1–5.
- [8] H. Chen, N. Li, R. Long, and Y.-C. Liang, "Channel estimation and training design for active ris aided wireless communications," *IEEE Wireless Communications Letters*, vol. 12, no. 11, pp. 1876–1880, 2023.
- [9] M. A. Haider, Y. D. Zhang, and E. Aboutanios, "Channel estimation and prediction in wireless communications assisted by semi-passive ris," in ICASSP 2024 - 2024 IEEE International Conference on Acoustics, Speech and Signal Processing (ICASSP), 2024, pp. 8601–8605.
- [10] Z. Zhang and W. Yu, "Codebook learning for active sensing with reconfigurable intelligent surface," in 2024 IEEE 25th International Workshop on Signal Processing Advances in Wireless Communications (SPAWC), 2024, pp. 821–825.
- [11] Y. Han, S. Jin, C.-K. Wen, and X. Ma, "Channel estimation for extremely large-scale massive mimo systems," *IEEE Wireless Communications Letters*, vol. 9, no. 5, pp. 633–637, 2020.
- [12] E. Björnson, J. Hoydis, L. Sanguinetti et al., "Massive mimo networks: Spectral, energy, and hardware efficiency," Foundations and Trends® in Signal Processing, vol. 11, no. 3-4, pp. 154–655, 2017.
- [13] M. Haghshenas, P. Ramezani, M. Magarini, and E. Björnson, "Parametric channel estimation with short pilots in ris-assisted near-and far-field communications," *IEEE Transactions on Wireless Communications*, vol. 23, no. 8, pp. 10366–10382, 2024.
- [14] H. Do and N. Lee, "Global optimization of active ris in linear time," in ICASSP 2024-2024 IEEE International Conference on Acoustics, Speech and Signal Processing (ICASSP). IEEE, 2024, pp. 8866–8870.
- [15] P. Ramezani and E. Björnson, "Near-field beamforming and multiplexing using extremely large aperture arrays," in *Fundamentals of 6G Commu*nications and Networking. Springer, 2023, pp. 317–349.